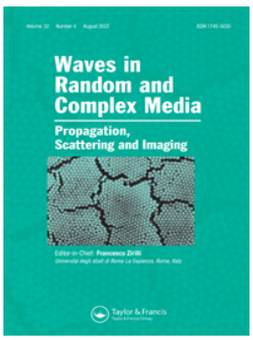

Taylor & Francis
Taylor & Francis Group

Waves in Random and Complex Media

ISSN: (Print) (Online) Journal homepage: https://www.tandfonline.com/loi/twrm20

Dynamism of a hybrid Casson nanofluid with laser radiation and chemical reaction through sinusoidal channels

Sara I. Abdelsalam, Kh. S. Mekheimer & A. Z. Zaher

To cite this article: Sara I. Abdelsalam, Kh. S. Mekheimer & A. Z. Zaher (2022): Dynamism of a hybrid Casson nanofluid with laser radiation and chemical reaction through sinusoidal channels, Waves in Random and Complex Media, DOI: 10.1080/17455030.2022.2058714

To link to this article: https://doi.org/10.1080/17455030.2022.2058714

WAVES IN RANDOM AND COMPLEX MEDIA
https://doi.org/10.1080/17455030.2022.2058714

Taylor & Francis
Taylor & Francis Group

Dynamism of a hybrid Casson nanofluid with laser radiation and chemical reaction through sinusoidal channels

Sara I. Abdelsalam[a], Kh. S. Mekheimer[b] and A. Z. Zaher[c]

[a]Basic Science, Faculty of Engineering, The British University in Egypt, Al-Shorouk City, Cairo, Egypt; [b]Mathematics Department, Faculty of Science, Al-Azhar University, Nasr City Cairo, Egypt; [c]Engineering Mathematics and Physics Department, Faculty of Engineering, Shubra-Benha University, Cairo, Egypt

ABSTRACT

This article studies the impact of laser radiation and chemical reaction with electromagnetic field and electroosmotic flow of hybrid non-Newtonian fluid via a sinusoidal channel. A mathematical model is used to simulate the arisen non-linear partial differential equations (PDEs). By employing the suitable transformations, the system of PDEs is then transformed to a non-linear system of ordinary differential equations (ODEs). The impact of the pertinent parameters on the pressure rise, velocity profile, streamlines and temperature distribution has been discussed. It has been noticed that the laser parameter enhances the fluid flow and the temperature distribution. This result occurs due to the impact of laser radiation that decreases the blood viscosity which in turn implies an increase in the fluid velocity leading to an enhancement in the heat transfer inside the fluid layers. The technique of laser radiation plays an important role in treating many viral and autoimmune diseases. The current study of radiation has the intention to help inhibit bacterial growth, increase oxygen binding to the blood, transport oxygen to organs and activate white blood cells.

ARTICLE HISTORY
Received 2 November 2021
Accepted 23 March 2022

KEYWORDS
Hybrid nanofluid; laser radiation; electroosmotic forces; electromagnetic effect; chemical reaction; heat transfer

1. Introduction

The practice of irradiation of blood outside the body began to spread in the 1920s with ultraviolet radiations. Such practices were initiated by Emmet Knott [1], who treated the contagious sicknesses in the blood using the properties of ultraviolet radiation germs. This approach has also been used to cure some autoimmune and aggressive diseases. The conclusions of this bloody radiation combined destroying and inhibiting bacterial germination, increasing oxygen linkage to the blood and transporting oxygen to body parts, dilatation of blood vessels, arousal of white blood cells, stimulating cellular immunity, lowering blood viscosity, improving microcirculation, decreasing platelet aggregation, etc. In the 1990s, some Russian scientists started using laser beams for injecting blood irradiation. For instance, Stulin et al. [2] recorded a fruitful treatment for vascular blood irradiation to the schizophrenic syndrome using a drug that is resistant to depression. These results were reported on the basis of the blood ability in destroying the active metabolic leukocytes. This experiment specified that laser beams are very effective in such situations. Dang Siposan

CONTACT Sara I. Abdelsalam sara.abdelsalam@bue.edu.eg

and Adalbert Lukacs [3] demonstrated the results of laser radiation (LR) on the blood components of humans in vitro and studied its effects on the blood that is separated from the vessels. They reported that the effects of LR could be beneficial in helping maintain blood, in the revitalization of saved blood and in the operation of stimulation of immunity in related syndromes. Laser treatments are further capable of stimulating intracellular biological responses, stimulating the production of adenosine triphosphate, nitric oxide and reactive oxygen species. It also facilitates the permeability of a membrane.

Nanomaterials have been of great interest to engineers as well as to scientists during the previous decades. As a matter of fact, nanomaterials are known to enhance the thermal conductivity of base fluids. The first one who suggested the addition of carbon nanotubes and solid particles in base fluids was Maxwell [4]. The results achieved were motivational, however, some problems were raised such as pressure drop enhancement and pipe erosion. Then, Choi [5] proposed the notion of carbon nanotubes and nanoscaled particles in base fluids and named them as nanofluids. Metals, such as Ag and Cu, and metal oxides, such as Al_2O_3 and CuO, are the most widely used nanoparticles. Improved nanofluids' thermal conductivity has important applications not only in domestic heating but also in heat exchangers and cooling systems. Nanofluids, discovered by Choi [6], are colloids composed of nanoparticles and base fluid. Nanoparticles have thermal conductivity, typically greater in magnitude than base fluids and significantly smaller in size than 100 nm. The work of nanoparticles greatly improves the heat transfer efficiency of the base fluids. Basic fluids can be water, synthetic liquids, fats, lubricants and blood. Nanoparticles are synthetic materials with substantial use in biomedicine because of the special manner in which they interact with matter. Another particular type of nanofluid is called hybrid nanofluid, these are formed by the suspension in the base fluid of two or more kinds of nanoparticles with hybrid nanoparticles. Suspended nanoparticles help improve fluid flow and heat transfer of the underlying fluid and chemical characteristics of different materials at the same time and has been commonly used in the production of anti-tumor medicines. Some studies that discuss nanofluids and hybrid nanofluids are reported in [7–18].

Fluid flow investigation in bio-microfluidic systems is implemented by the electroosmosis process. The latter is the principal instrument for the stream activation in a wide scope of utilization. This electroosmotic transition takes place in such a way that, as long as the polar outer layer is connected to the electrolyte device, the counterparts of the electrolyte should be allowed to pass through the surface of the capacitor and ultimately to build a membrane with a high convergence of counteractors, which is commonly named after the Stern layer. In addition to the exterior diffuse coat, the electric double layer (EDL) is produced in the area of the charged board. Applying the ambient electrical field to the electroosmotic flow (EOF), the functional particles in the dispersed area of the EOF are induced to travel and accomplish fluid displacement, which is typically known as the 'EOF'. Propelled by the monumental use of the stream of the electro-assimilation, various experiments are investigated [19–23].

Another significant nonmechanical micropump is the electromagnetohydrodynamic (EMHD) which has different applications, some of which are fluid mixing and pumping along with flow control in microfluidic systems [24–26]. Lorentz force is generated because of an electric field force applied across the channel in the presence of a perpendicular magnetic field force. The integration between latter fields is known as the electromagnetic forces. In comparison to the various types of non-mechanical micropumps, the EMHD

micropumps have a range of points of concern, specifically simple production processes, bidirectional siphoning ability and consistent flow power.

Motivated with the aforesaid discussion, our aim is to study laser radiation effects on the peristaltic flow of non-Newtonian hybrid nanofluid with the electroosmotic effect and the electric field that occurs due to the application of a magnetic field. The corresponding numerical and analytical approaches are used to determine the physical parameters of the system according to sufficient constraints. The contribution of the related parameters will be addressed graphically.

In this research, Section 1 represents the introduction, Section 2 presents the mathematical formulation, Section 3 shows the mathematical method as well the appropriate analytical solutions to the problems, while Section 4 includes the discussion and results. Last, Section 5 shows the limitations of our article and summarizes the main points.

2. Mathematical formulation

Consider an EMHD and electroosmotic flow of a hybrid non-Newtonian nanofluid with heat transfer transient through a two-dimensional conduit. The movement in the channel is stimulated by imposing sinusoidal traveling waves of reasonable amplitude on the compliant walls of the channel. The flow is triggered by the Lorenz force, $\vec{j} \times \vec{B}$, that is produced by two fields (magnetic field $\vec{B}(0, B_0, 0)$ and electric field $\vec{E}(0, 0, E_0)$). The current density for the nanofluid is known as $\vec{j} = \sigma^*(\vec{E} + \vec{V} \times \vec{B})$ and the velocity is known as $\vec{V}(\bar{u}, \bar{w})$. The geometry of the channel wall is mathematically given by

$$y = \pm \left(d + a \sin \frac{2\pi}{\lambda}(x - ct) \right)$$

where d is the channel mean-half width, λ is the wavelength, t is the time, a is the amplitude and c is the phase speed of the wave, see Figure 1.

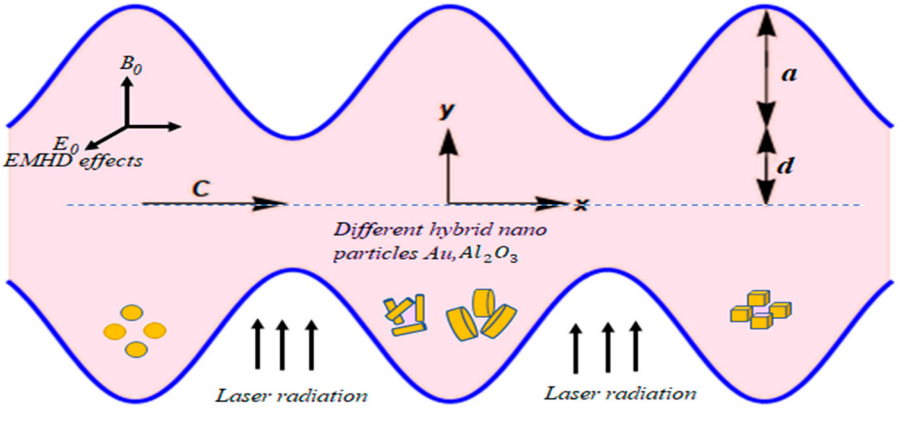

Figure 1. Schematic diagram of the problem.

2.1. Electroosmotic flow

The density of charge ρ_e in the fluid per a unit volume is known as

$$\rho_e = \varepsilon e(n^+ - n^-) = -2\varepsilon e n_0 \sinh\left\{\frac{\varepsilon e\bar{\varphi}}{k_B T_{av}}\right\}, n^- = n_0 e^{\frac{\varepsilon e\bar{\varphi}}{k_B T_{av}}}, n^+ = n_0 e^{\frac{-\varepsilon e\bar{\varphi}}{k_B T_{av}}}. \tag{1}$$

where $\varepsilon$is the valence of ions, n^+ and n^- are, respectively, the density numbers of the positive and negative ions, e is the charge of electron, k_B Boltzmann constant and T_{av} is the local absolute temperature of the electrolytic solution and n_0 is the bulk volume concentration for the positive or negative ions.

By making use of the principle of Debye–Huckel linearization $\{\varepsilon e\varphi'/k_B T_{av} \ll 1\}$, Equation (11) reduces to

$$\rho_e = \frac{-\epsilon}{K^2}\bar{\varphi}, \tag{2}$$

where $K = (\varepsilon e)^{-1}(\epsilon k_B T_{av}/2n_0)$ is Debye–Huckel's parameter that describes the thickness properties of the EDL. The electroosmotic potential distribution can be attained by utilizing the Poisson–Boltzmann equation:

$$\frac{\partial^2\bar{\varphi}}{\partial\bar{x}^2} + \frac{\partial^2\bar{\varphi}}{\partial\bar{y}^2} = \frac{1}{K^2}\bar{\varphi}, \tag{3}$$

where $\bar{\varphi}$ and ϵ are, respectively, the electroosmotic potential function and the dielectric constant.

2.2. Non-Newtonian Casson fluid equation

The isotropic rheological equation of the Casson fluid statement for the incompressible flow is given by

$$\tau_{ij} = \begin{Bmatrix} 2e_{ij}\left(\mu_B + \frac{P_y}{2\mu}\right), \pi < \pi_{e,} \\ 2e_{ij}\left(\mu_B + \frac{P_y}{2\mu}\right), \pi < \pi_e. \end{Bmatrix} \tag{4}$$

Here, P_y is the fluid stress, π represents the product of the deformation rate component with itself $(= e_{ij}e_{ij})$, π_e is the product critical value on the basis of the given non-Newtonian model, e_{ij} is the (i,j)th deformation rate component and μ_B is the plastic viscosity of the fluid. It is worth noting that the current system reduces to a Newtonian one when the yield stress vanishes, i.e. when $P_y = 0$.

2.3. Governing equation with laser radiation

The governing equations for mass, motion, heat conservation and concentration for the 2D unsteady flow of incompressible Casson fluid with electromagnetic field, electroosmotic

flow, laser radiation and chemical radiation are given by [16,17,27]:

$$\frac{\partial \bar{u}}{\partial \bar{x}} + \frac{\partial \bar{v}}{\partial \bar{y}} = 0, \tag{5}$$

$$\rho_{hnf}\left(\frac{\partial \bar{u}}{\partial \bar{t}} + \bar{u}\frac{\partial \bar{u}}{\partial \bar{x}} + \bar{v}\frac{\partial \bar{u}}{\partial \bar{y}}\right) = -\frac{\partial \bar{P}}{\partial \bar{x}} + \mu_{hnf}\left[\frac{\partial \tau_{xx}}{\partial \bar{x}} + \frac{\partial \tau_{xy}}{\partial \bar{y}}\right] + \sigma E_0 B_0 - \sigma {B_0}^2 \bar{u} + \rho_e E_z + (\rho\gamma)_{hnf} g(T - T_0), \tag{6}$$

$$\rho_{hnf}\left(\frac{\partial \bar{v}}{\partial \bar{t}} + \bar{u}\frac{\partial \bar{v}}{\partial \bar{x}} + \bar{v}\frac{\partial \bar{v}}{\partial \bar{y}}\right) = -\frac{\partial \bar{P}}{\partial \bar{x}} + \mu_{hnf}\left[\frac{\partial \tau_{yx}}{\partial \bar{x}} + \frac{\partial \tau_{yy}}{\partial \bar{y}}\right], \tag{7}$$

$$(\rho C)_{hnf}\left(\frac{\partial T}{\partial \bar{t}} + \bar{u}\frac{\partial T}{\partial \bar{x}} + \bar{v}\frac{\partial T}{\partial \bar{y}}\right) = k_{hnf}\left(\frac{\partial^2 T}{\partial \bar{x}^2} + \frac{\partial^2 T}{\partial \bar{y}^2}\right) + I_0 \Omega_0 e^{-\Omega_0 \bar{y}} - \frac{\partial q_r}{\partial \bar{y}}, \tag{8}$$

where $(\bar{u}, \bar{v})$ are the components of velocity, ρ_e is the density of charge, σ the electrical conductivity, μ_{hnf} is the viscosity of the hybrid nanofluid, k_{hnf} is the hybrid nanofluid thermal conductivity, ρ_{hnf} is the hybrid nanofluid density, $(\rho C)_{hnf}$ is the heat capacitance of hybrid nanofluid, I_0, Ω_0 are the laser radiation and γ is the thermal expansion coefficient.

According to the Rosseland approximation [28,29], the radiative heat flux takes the following form:

$$q_r = -\frac{4}{3}\frac{\sigma'}{k}\frac{\partial T^4}{\partial y},$$

such that σ' is the constant of Stefan–Boltzmann and k is the coefficient of mean absorption.

Since the difference in temperature through fluid flow is small, then T^4, using Taylor series, can be written as follows:

$$T^4 = {T_0}^4 + 4{T_0}^3(T - T_0) + 6{T_0}^2(T - T_0)^2 + \ldots,$$

Neglecting the higher order terms with respect to $(T - T_0)$, we get

$$T^4 = 4{T_0}^3 T - 3{T_0}^3.$$

The blood thermophysical properties with nanofluid model are given by [30,31]

$$\rho_{nf} = \rho_f\left(1 - \phi + \phi\left(\frac{\rho_s}{\rho_f}\right)\right), (\rho C)_{nf} = (\rho C)_f\left(1 - \phi + \phi\left(\frac{(\rho C)_s}{(\rho C)_f}\right)\right),$$
$$(\rho\gamma)_{nf} = (\rho\gamma)_f\left(1 - \phi + \phi\left(\frac{(\rho\gamma)_s}{(\rho\gamma)_f}\right)\right), \frac{\mu_{nf}}{\mu_f} = \frac{1}{(1-\phi)^{2.5}},$$
$$\frac{k_{nf}}{k_f} = \frac{k_s + 2k_f - 2\phi(k_f - k_s)}{k_s + 2k_f + \phi(k_f - k_s)}. \tag{9}$$

where the thermophysical properties for the hybrid blood nanofluid can be written as

$$\begin{aligned} M &= \frac{1}{(1-\phi_{s1})^{2.5}(1-\phi_{s2})^{2.5}};\\ (\rho\gamma)_{hnf} &= (\rho\gamma)_f\left((1-\phi_{s2})\left((1-\phi_{s1})+\phi_{s1}\frac{(\rho\gamma)_{s1}}{(\rho\gamma)_f}\right)+\phi_2\frac{(\rho\gamma)_{s2}}{(\rho\gamma)_f}\right),\\ \frac{k_{hnf}}{k_{bf}} &= \frac{k_{s2}+(n-1)k_f-(n-1)\phi_{s2}(k_f-k_{s2})}{k_{s2}+(n-1)k_f+\phi_{s2}(k_f-k_{s2})},\\ \frac{k_{bf}}{k_f} &= \frac{k_{s1}+(n-1)k_f-(n-1)\phi_{s1}(k_f-k_{s1})}{k_{s1}+(n-1)k_f+\phi_{s1}(k_f-k_{s1})}. \end{aligned} \tag{10}$$

such that ϕ_{s1} and ϕ_{s2} are the volume fraction for Au and Al_2O_3 nanoparticles respectively.

2.4. Non-dimensional physical parameters

Introducing the transformation between the wave frame (x, y) and laboratory frame (X, Y) in order to facilitate the solutions:

$$x = X - ct, \quad y = Y, \quad u = U - c, \quad p = P. \tag{11}$$

Introducing the following dimensionless parameters:

$$\begin{aligned} &u = \frac{\bar{u}}{c}, x = \frac{\bar{x}}{\lambda}, y = \frac{\bar{y}}{a}, v = \frac{\bar{v}}{\delta c}, p = \frac{a^2}{\lambda c\mu_f}\bar{p}, \delta = \frac{a}{\lambda}, \vartheta = \frac{\bar{\varphi}}{\zeta}, Re = \frac{\rho_f ca}{\mu_f}, E_s = \frac{aE_0}{c}\sqrt{\frac{\sigma}{\mu_f}},\\ &Ha = aB_0\sqrt{\frac{\sigma}{\mu_f}}, Gr = \frac{(\rho\gamma)_f ga^2(T_1-T_0)}{\mu_f c}, \theta = \frac{T-T_0}{T_1-T_0}, Rn = \frac{16}{3}\frac{\sigma'}{k\mu_f c_f}{T_0}^3. \end{aligned} \tag{12}$$

By employing suppositions, small Reynolds number and long wavelength, Equations (5)–(8) become

$$0 = -\frac{\partial p}{\partial \bar{x}} + \frac{\mu_{hnf}}{\mu_f}\left[1+\frac{1}{\beta}\right]\frac{\partial^2 u}{\partial y^2} + E_S Ha - Ha(u+1) + m^2 U_{HS}\vartheta(y) + \frac{(\rho\gamma)_{hnf}}{(\rho\gamma)_f}Gr\theta(y) \tag{13a}$$

$$0 = -\frac{\partial p}{\partial y}, \tag{13b}$$

$$0 = \frac{k_{hnf}}{k_f}(1+Rnpr)\frac{\partial^2\theta}{\partial y^2} + Da\gamma^* e^{-\Omega^* y}, \tag{13c}$$

$$\frac{\partial^2\vartheta}{\partial y^2} = m\vartheta, \tag{13d}$$

where γ^* and Ω^* are the laser parameters, Da is the electrical Raleigh number, β is the non-Newtonian fluid parameter, Rn is the parameter of chemical reaction, m is the electroosmotic parameter, Es is the parameter of electrical field strength, Ha is the Hartmann number and UHs is the Helmholtz–Smoluchowski velocity (i.e. maximum velocity of electroosmosis).

The boundary conditions at the walls in the fixed frame are

$$U = 0, T = T_0, \bar{\varphi} = \zeta \text{ at } y = h(x),$$
$$U = 0, T = T_1, \overline{\varphi} = \zeta \text{ at } y = -h(x,t). \tag{14a}$$

The corresponding dimensionless boundary conditions, in the wave frame, become

$$u = -1, \theta = 1, \vartheta = 1 \text{ at } y = h(x),$$
$$u = -1, \theta = 0, \vartheta = 1 \text{ at } y = -h(x). \tag{14b}$$

3. Model solution

By making use of the boundary conditions that are given by Equation (14b), Equations (13) can be written as

$$\vartheta(y) = \frac{\cosh(my)}{\cosh(mh)}, \tag{15a}$$

$$\begin{aligned}\theta(y) = {} & \frac{e^{-\Omega^*(h+y)}}{2hm^2(k^*+Rn)}(-2e^{h(y)\Omega^*}Da\Omega^* h(y) + e^{\Omega^*(2h+y)}Da\Omega^*(h-y) \\ & + e^{\Omega^*(h+y)}\Omega^{*2}(k^*+Rn)(h-y) + e^{\Omega^* y}Da\Omega^*(h+y)),\end{aligned}$$

$$\begin{aligned}u(y) = {} & \frac{U_{Hs}}{(Ha^2-\mu^* m^2)}\left(-\frac{\cosh\left(\sqrt{\mu^*}Ha\,y\right)}{\cosh\left(\sqrt{\mu^*}Ha\,h\right)} + \frac{\cosh m\,y}{\cosh m\,h}\right) \\ & - e^{-\beta y}\left(-2e^{\beta y}h\Omega^{*2}(-(Ha^2-\Omega^{*2}\mu^*)((\rho\gamma)^* Gr + 2(Es\,Ha + Ha^2 - p))(k^*+Rn)\right. \\ & + 2Da\Omega^*(\rho\gamma)^* Gr\mu^* \cosh(\Omega^* h))\cosh\left(\sqrt{\mu^*}Ha\,y\right)\sinh\left(\sqrt{\mu^*}Ha\,h\right) \\ & + \sinh\left(2\sqrt{\mu^*}Ha\,h\right)(\cosh(\beta y)(2Da\Omega^*(\rho\gamma)^* Gr\,h\,Ha^2 \\ & + \Omega^{*2}(-Ha^2+\Omega^{*2}\mu^*)(k^*+Rn)((\rho\gamma)^* Gr\,h + 2Es\,h\,Ha - 2\,h\,p - G\,y) \\ & + 2Da\Omega^*(\rho\gamma)^* Gr(Ha^2-\Omega^{*2}\mu^*)(-h\cosh(\Omega^* h) + y\sinh(\Omega^* h))) \\ & + (-2Da\Omega^*(\rho\gamma)^* Gr\,h\,Ha^2 + \Omega^{*2}(-Ha^2+\Omega^{*2}\mu^*)(k^*+Rn)((\rho\gamma)^* Gr\,h \\ & + 2Es\,hHa - 2\,h\,p - G\,y) \\ & + 2Da\Omega^*(\rho\gamma)^* Gr(Ha^2-m^2\mu^*)(-h\cosh(\Omega^* h) + y\sinh(\Omega^* h)))\sinh\beta y) \\ & + 2e^{\beta y}(\rho\gamma)^* Gr\,h\Omega^{*2}\cosh\left(\sqrt{\mu^*}Ha\,h\right)((-Ha^2+\Omega^{*2}\mu^*)(k^*+Rn) \\ & \left. + 2Da\Omega^*\mu^*\sinh(\Omega^* h))\sinh\left(\sqrt{\mu^*}Ha\,y\right)\right),\end{aligned} \tag{15b, 15c}$$

where $\mu^* = \mu_{hnf}/\mu_f, k^* = k_{hnf}/k_f, (\rho\gamma)^* = (\rho\gamma)_{hnf}/(\rho\gamma)_f$, and $\beta = \Omega^*/2$.

Table 1. Thermophysical characteristics.

	Fluid phase (F)	Solid nanoparticle phase (S)	
Physical properties	Blood	Au	Al_2O_3
ρ(kg/m^3)	1063	19, 300	3970
k(W/mK)	0.492	400	40
γ(1/K)	0.18	1.42	8.9

3.1. Rate of volume flow and pressure rise

The appropriate dimensionless physical forms for the volume flow rate and the pressure rise may be defined as

$$F = 2\int_0^{h(x)} u(y)dy, \tag{16}$$

$$\Delta p = \int_0^1 \left(\frac{dp}{dx}\right) dx. \tag{17}$$

4. Limitations

Laser radiation and chemical reaction with peristaltic mechanism for a non-Newtonian hybrid nanofluid with the electroosmotic effect and the electric field is investigated. The movement in the channel is stimulated by imposing sinusoidal traveling waves of reasonable amplitude on the walls of the channel. There are limitations associated with this study which needs to be discussed here:

- The analysis uses a plane of two-dimensional model.
- The theoretical analysis begins with the most general form of the Navier–Stokes equation for fluid motion and is followed with some assumptions to solve these equations.
- Long wavelength approximation is considered $\delta = a/\lambda << 1$ in our results and with small Reynolds number $Re = \rho_f ca/\mu_f$.
- Thermophysical characteristics for nanofluids and hybrid nanofluids are considered in Table 1 with specific shapes (spheres, bricks, cylinders).
- The principle of Debye–Huckel linearization $K = (\varepsilon e)^{-1}(\epsilon k_B T_{av}/2n_0) \ll 1$ is taken into consideration.
- The difference in temperature through fluid flow is small, so that $T^4 = 4{T_0}^3 T - 3{T_0}^3$.

5. Results and discussion

Detailed schematic frameworks have been determined with the help of arithmetic calculations to obtain closed-form solutions that express the proposed hemodynamic velocity and propagation of temperature through the stream. A study was conducted to address the impact of chosen parameters on the blood vessel section with the effect of laser radiation and chemical reaction. Particularly, we investigate the impact of laser parameters

Table 2. Shapes of nanoparticles with their shape factors.

Nanoparticle shapes	Shape factor
Spheres	3
Bricks	3.7
Cylinders	4.9
Platelets	5.7

Ω^* and γ^*, electrical Raleigh number *Da*, non-Newtonian fluid parameter β, chemical reaction parameter *Rn*, electroosmotic parameter *m*, the electrical field strength parameter *Es*, the Hartmann number *H a* and the Helmholtz–Smoluchowski velocity *UHs*. We use the MATHEMATICA software so that we compute the pressure rise numerically. We have also established a comparison between the hybrid nanofluid and nanofluid. The thermophysical data for the basic thermal power, thermal conductivity and density of the blood with Au and Al_2O_3 nanoparticles are given in Table 1 [6,31]. The shapes of the nanoparticles with their corresponding factors of shape are also seen in Table 2 [31].

5.1. Hemodynamic blood velocity

Figures 2–7 are graphed to discuss the effect of different parameters (Ω^*, γ^*, *Da*, β, *Rn*, *m*, *Es*, *Ha*, and *UHs*) on the velocity behavior. From Figure 2, it is found that when the laser parameters, Ω^*andγ^*, are reduced in the blood viscosity, the fluid velocity is enhanced. Also, it is shown that when $\Omega^* = 0$, the velocity, $u(y)$, behaves symmetrically and by enhancing the value of the laser parameter, the behavior is reversed. In Figure 3, the effect of electric Raleigh number is presented where we find that an increment of electric Raleigh number increases the blood velocity. This is because the effect of *Da* that reduces the density of the fluid causes the liquid particles to move freely, and this leads to an increase in the flow of fluid. As shown in Figure 4, the hemodynamic velocity of the nanofluid and hybrid nanofluid is compared. It is seen that the hemodynamic distribution of velocity of the hybrid nanofluids is greater than that of a nanofluid, which in turn means that mixed nanofluids are more beneficial in the medical pumps to deliver the drug. It also appears that the increase in the non-Newtonian parameter causes an increase in the speed of blood circulation. Figure 5 elucidates the hemodynamic velocity distribution for sundry values of heat radiation (chemical reaction). It is depicted that the uniform chemical reaction causes the flow to decelerate. This physical influence is due to the cumulative effect of the ratio of buoyancy between species, thermal diffusion and the frequency of the chemical reaction. Also, it is found that velocity behavior curves are converged with the increase of chemical reaction. From Figure 6, it is seen that as the magnetic field is increased, the hemodynamic velocity is reduced, i.e. as *Ha* increases the braking Hartmann number grows and that can be considered as an increment in the magnetic viscosity, consequently, the fluid moves as a whole mass of constant velocity. In Figure 7, it is observed that the hemodynamic velocity distribution increases by an increase in *Es*, *m*, and *UHs*. Figure 7(d) presents the effect of nanoparticles' different forms on hemodynamic motion. One may report that the velocity of spherical nanoparticles reduces relative to that of rods, bricks and platelet-shaped nanoparticles.

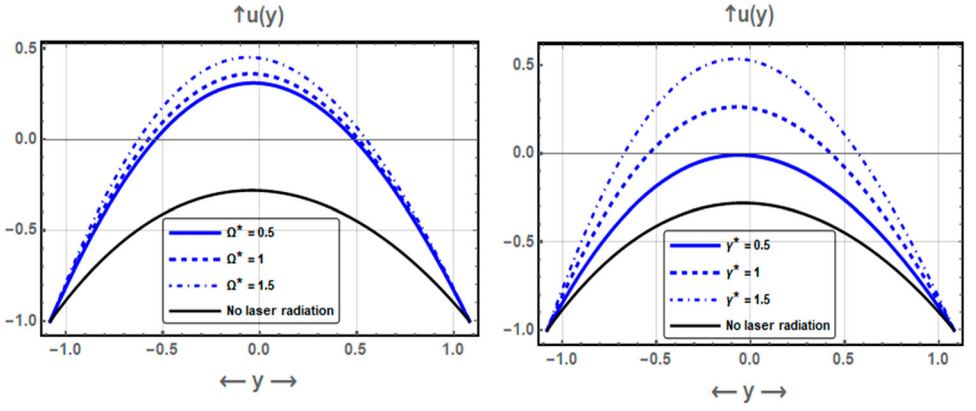

Figure 2. Variation of velocity component vs. y for different values of Ω^* and γ^*.

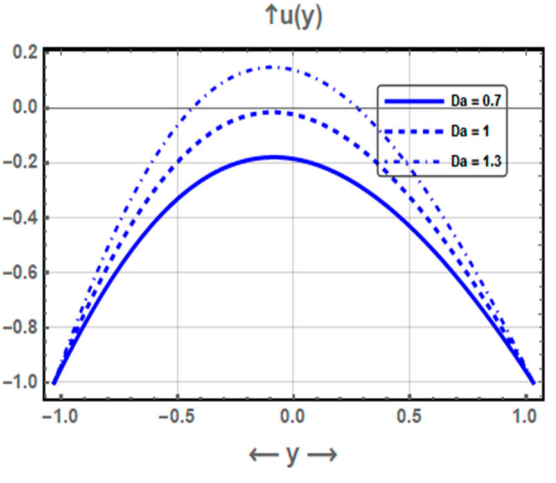

Figure 3. Variation of velocity component vs. y for different values electrical Raleigh number Da.

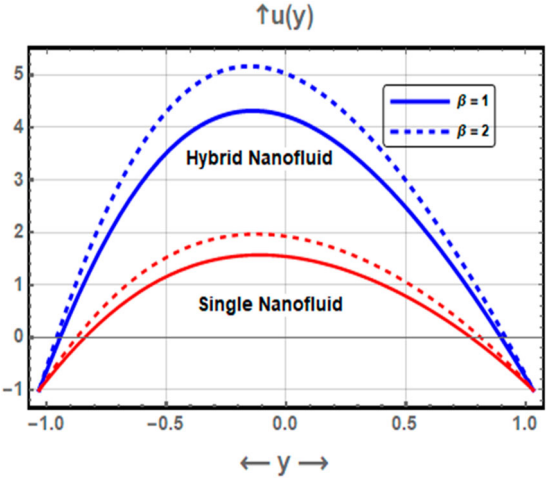

Figure 4. Variation of velocity component vs. y for different values non-Newtonian parameter β.

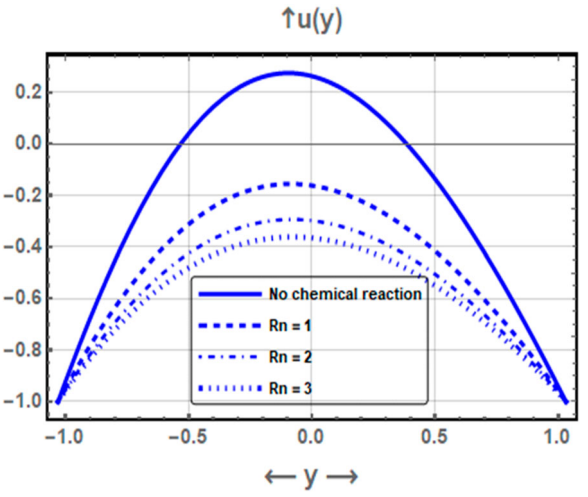

Figure 5. Variation of velocity component vs. *y* for different values electrical Raleigh number *Da*.

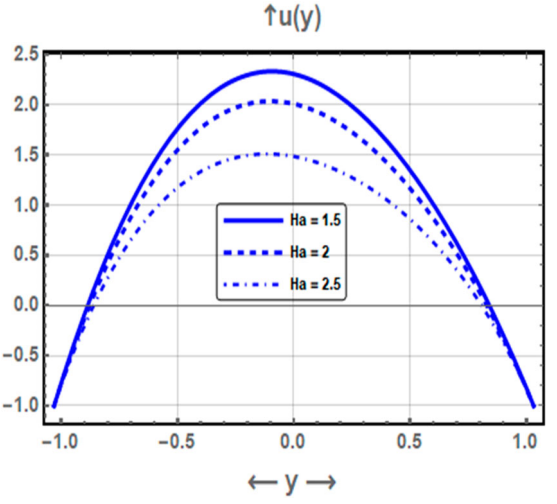

Figure 6. Variation of velocity component vs. *y* for different values non-Newtonian parameter β.

5.2. Trapping mechanism

The mechanism of trapping is an important aspect of hydrodynamic properties in aneurysm and stenosis. Trapped bolus can better be thought of through plotting contours. The system of trapping is transmitted by the circulating bolus internally. The volume of the flowing bolus through the fluid is surrounded with the streamlines. The trapping for $\Omega^*$and γ^*, *Da*, *Rn*, *m*, *Es*, *Ha* and *UHs* is discussed in Figures 8–15. In Figures 8 and 9, it is found that as Ω^* and γ^* increase, the number of the circulating bolus increases in the flow. Figure 10 studies the effect of *Da* where it is seen that an increment in *Da* implies an increase in the size and number of the circulating bolus in the lower channel and to a decrease in the size of the bolus in the upper region of the channel. From Figure 11, it is found that an increment in

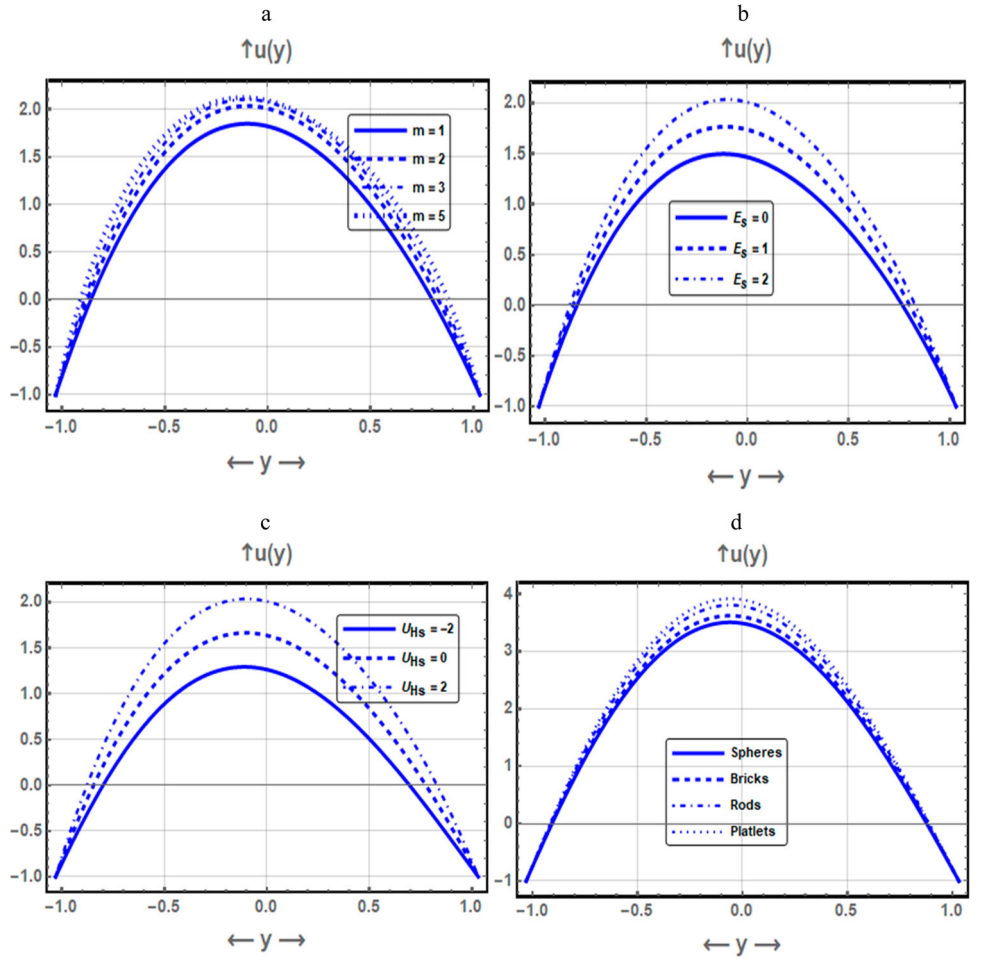

Figure 7. Variation of velocity component vs. *y* for different values of m (panel a), E_S (panel h), U_{HS} (panel c), and different shape of nanoparticles n (panel d).

Ha reduces the size and the number of the circulating bolus and the blood fluid moves as a bulk. Figure 12 describes the effect of chemical reaction parameter on the streamlines. It is seen that as the chemical reaction increases, the number and size of the fluid bolus decrease. As shown in Figures 13 and 14, the increase of *Es* and *UHs* implies an increase in the number of circulating bolus in the lower area of the channel. An opposite behavior is found in the upper region of the channel. Figure 11 describes the effect of the chemical reaction parameter on the streamlines, it is seen that as the chemical reaction increases, the number and size of the fluid bolus are reduced.

5.3. Pumping properties

Pressure rise is an important mechanism in a human body that supports movement of various biofluids (i.e. transport of urine, cilia motion, blood pumping, etc.). In biomedical engineering, various ways are developed on the basis of the phenomenon of stenosis

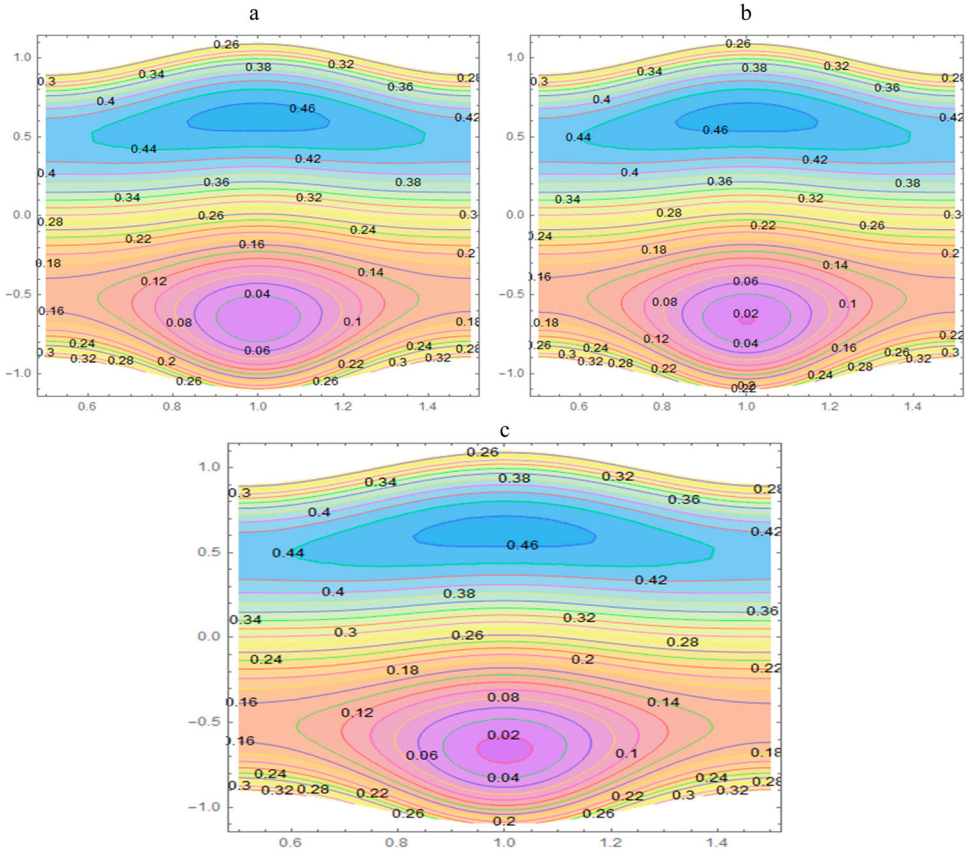

Figure 8. Streamlines for different values of Ω^* ($= 0.1, 0.3$, and 0.5 in panels a, b, and c respectively).

pumping. Figure 15 indicates the pressure increase versus z for various values of Ω^*, γ^*, Da, β, Rn, m, Es, Ha and UHs. These plots are broken down into four zones i.e. peristaltic pumping $\Delta p > 0; Q > 0$, retrograde pumping $\Delta p > 0; Q < 0$, co-pumping $\Delta p \langle 0; Q \rangle 0$ and free pumping $\Delta p < 0; Q < 0$. It can be seen from Figures 15(a,b) that as Ω^*andγ^* increase, the pressure rise increases. A different effect is seen in Figures 15(c,d) with an enhancement in the chemical reaction and electroosmotic parameter. In Figure 15(e), a comparison is made among nanofluid and hybrid nanofluid. The rise in pressure for hybrid nanofluid is seen to be greater than that of nanofluid which is physically beneficial for drug delivery. Also, in this Figure 15(e), it is seen that the rise in pressure is increased with an increase in U_{HS}. In Figure 15(f), a Casson parameter is studied, it is found that Δp increases in the region of retrograde pumping and decreases in the regions of peristaltic pumping and free pumping. As seen in Figure 15(g), as electrical Raleigh increases, the pressure rise increases.

5.4. Temperature distribution

Figure 16 is plotted to investigate the behavior of heat transport with y for sundry values of the Ω^* and γ^*, Da, Rn and n. A comparison is made for the nanofluid versus the hybrid nanofluid. It is observed from Figures 16(a,b) that an increment in Ω^* and γ^* implies to an

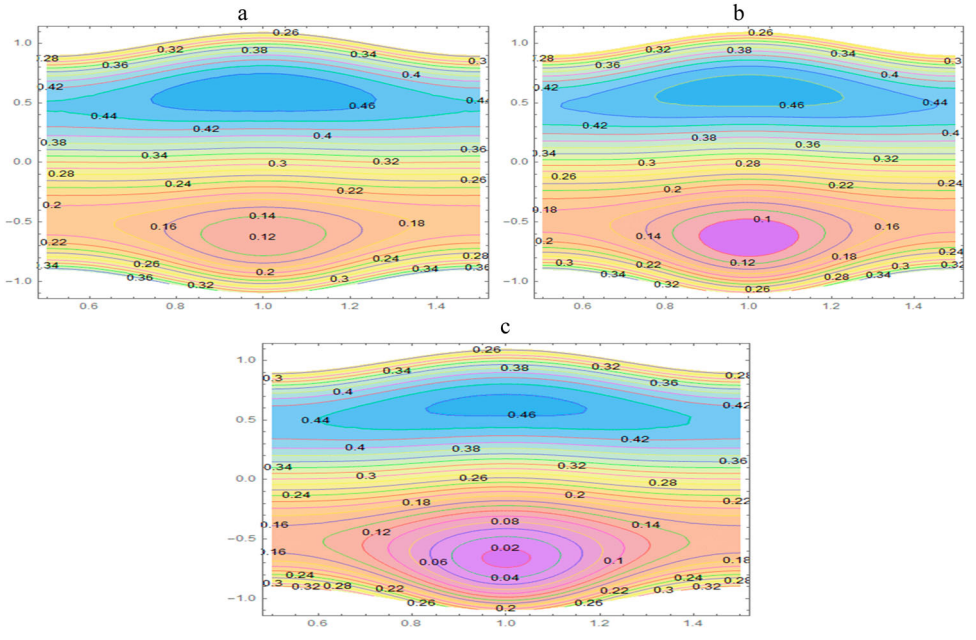

Figure 9. Streamlines for different values of γ^* ($=$ 0.5, 1, and 1.5 in panels a, b, and c respectively).

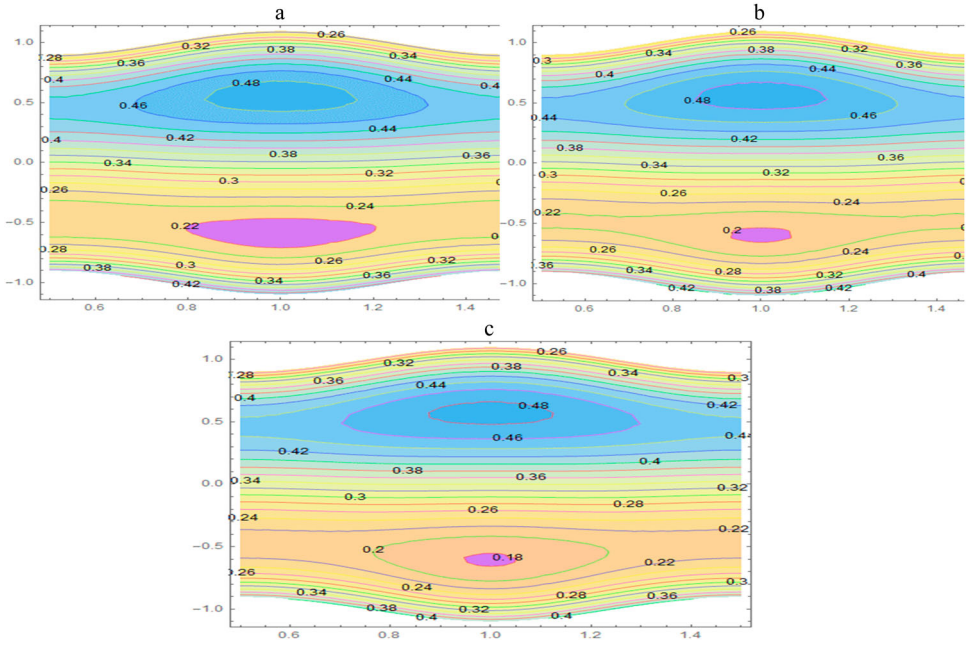

Figure 10. Streamlines for different values of *Da* ($=$ 0.1, 0.3, and 0.6 in panels a, b, and c respectively).

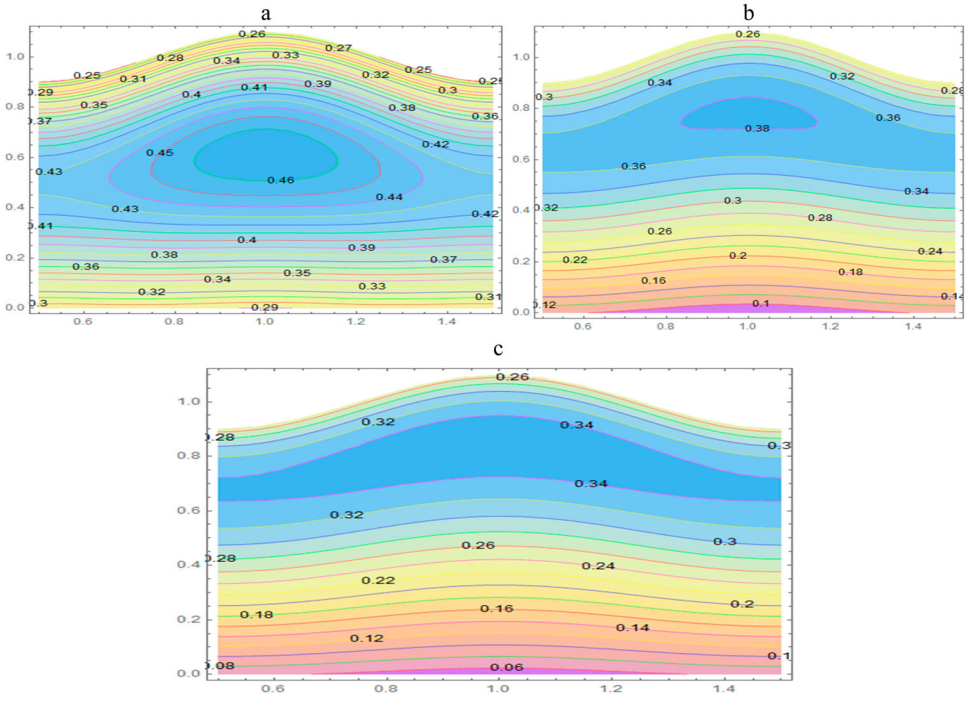

Figure 11. Streamlines for different values of *Ha* (= 3, 5, and 10 in panels a, b, and c respectively).

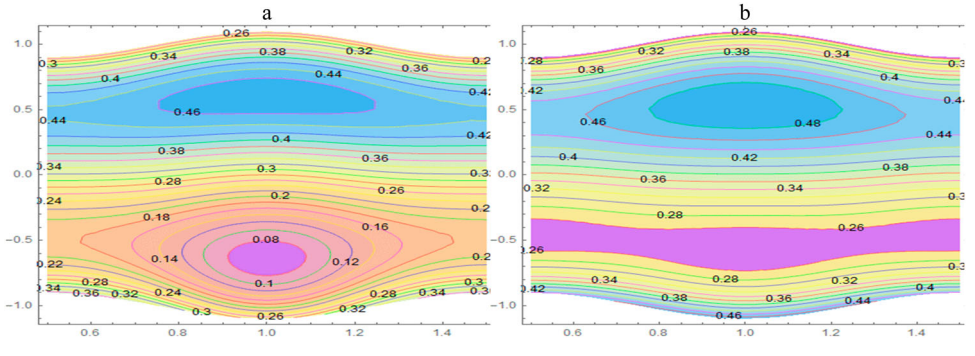

Figure 12. Streamlines for different values of *Rn* (= 0 and 5 in panels a and b, respectively).

enhancement in the heat transfer. This is because the laser parameters reduce the blood viscosity, and, consequently, the fluid velocity increases causing a rise in the heat transfer. This result is very interesting in treating many viral and autoimmune diseases. In Figure 16(c), it is observed that the heat transfer is greater for hybrid nanofluid when compared to a nanofluid. This last approach recognizes that hybrid nanofluid improves the thermal conductivity in a fluid that helps to destroy the virus or tumors. It is also found that an enhancement in *Da* results in an increase in the fluid heat transport. It is observed from Figure 16(d) that the chemical reaction decreases the heat transfer in the blood flow. From Figure 16(e), it is seen that the temperature is reduced for spherical nanoparticles than that of the other shapes of nanoparticles such as bricks, platelets and rods.

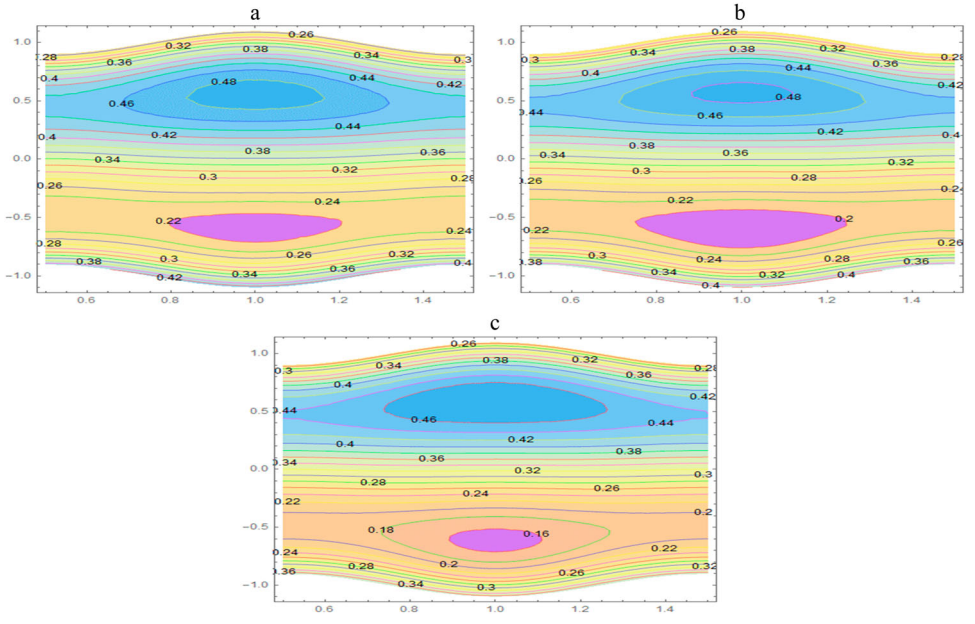

Figure 13. Streamlines for different values of E_S ($=$ 2, 2.5 and 3 in panels, a, b and c, respectively).

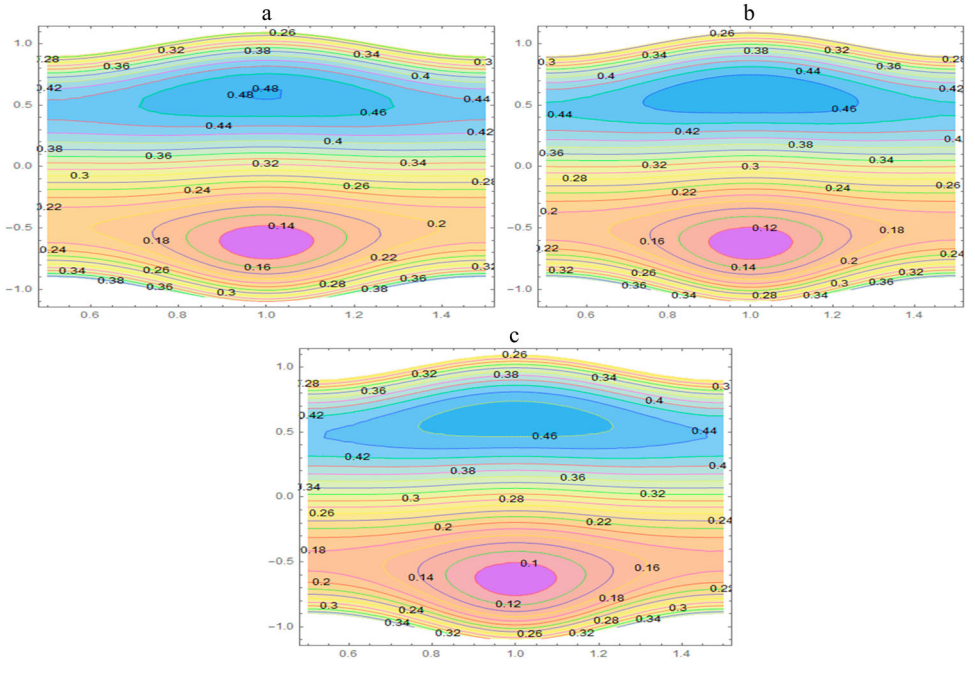

Figure 14. Streamlines for different values of U_{HS} ($=$ −2, 0 and 2 in panels, a, b and c, respectively).

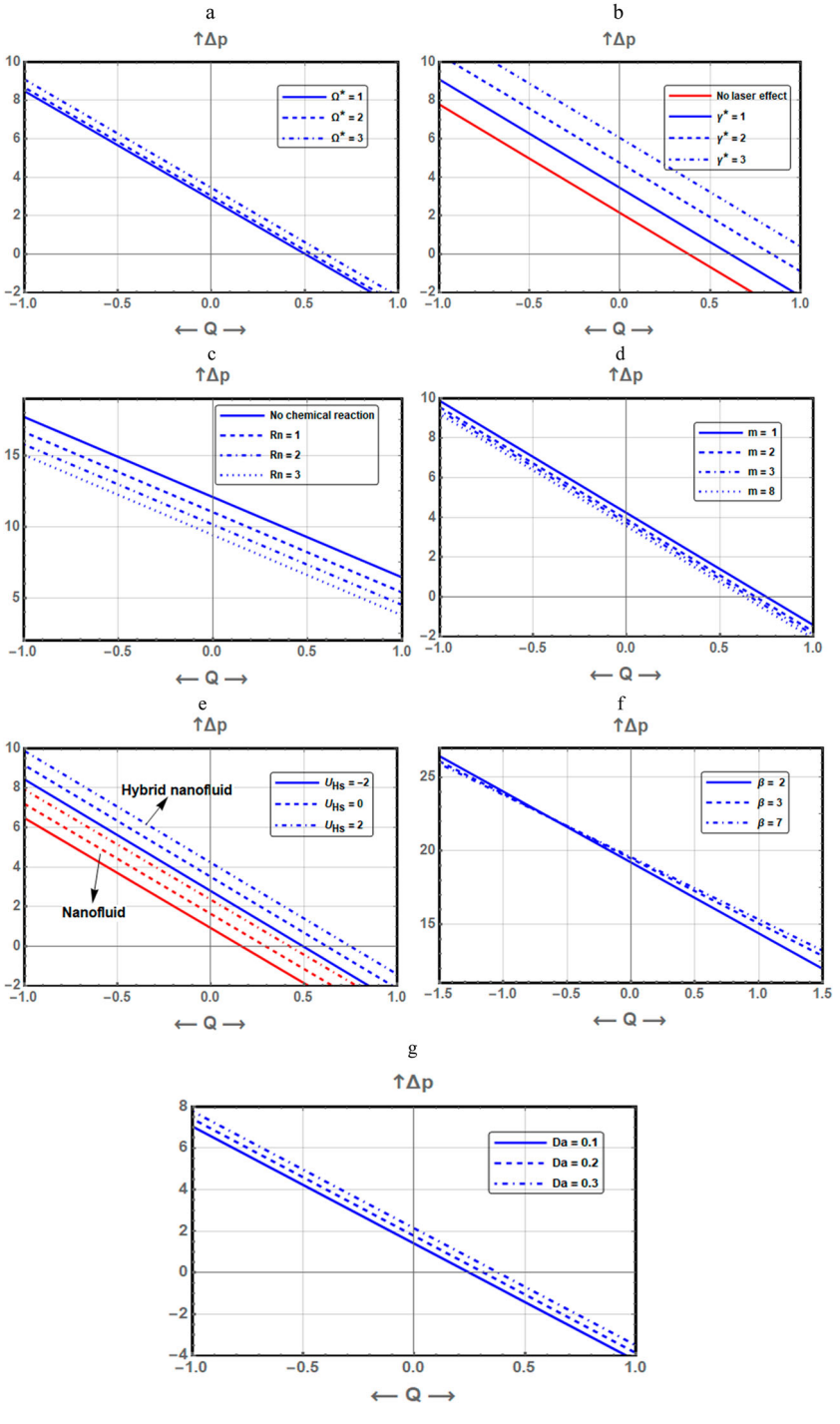

Figure 15. Variation of pressure rise vs. Q for different values of Ω^* (panel a), γ^* (panel b), Rn (panel c), m (panel d), U_{HS} (panel e), β (panel f), and Da (panel f).

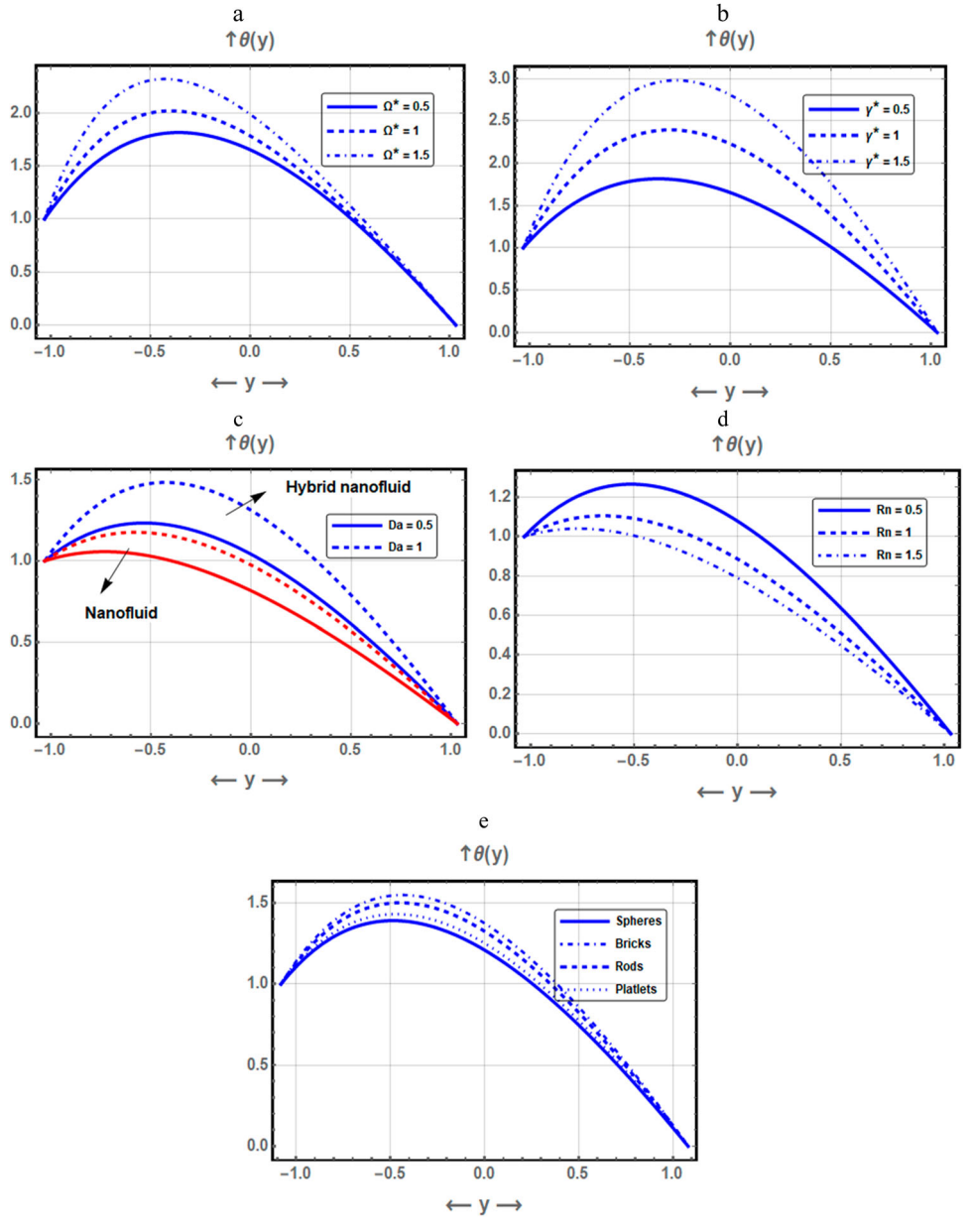

Figure 16. Variation of heat transfer vs. y for different values of Ω^* (panel a), γ^* (panel b), U_{HS} (panel c), Rn (panel d), and n nanoparticles shapes (panel e).

6. Concluding remarks

In this work, we investigate laser radiation with the peristaltic mechanism for a non-Newtonian hybrid nanofluid with the electroosmotic effect and the electric field. Solutions are derived to investigate the effects of the physical parameters of interest. Research has

been performed to examine the impact of selected structural properties. The impact of the pertinent parameters is explored graphically. The main findings are found as follows:

I. The mixed nanofluids are useful in the medical pumps of the delivery of drugs since the hemodynamic velocity of the hybrid nanofluid is greater than that of a nanofluid.
II. The flow decelerates in the presence of a uniform chemical reaction.
III. The electroosmotic parameter, electrical field strength parameter and maximum electro-osmotic velocity have an increasing effect on the hemodynamic velocity.
IV. Unlike the effect of the electrical Raleigh parameter *Da* on the trapped bolus in the upper region of the conduit, *Da* tends to increase the size and number of circulating bolus in the lower region.
V. As the chemical reaction increases, the number and size of the circulating bolus of the fluid decrease.
VI. The heat transfer is smaller for a nanofluid than that of a hybrid nanofluid.
VII. The temperature is reduced for spherical nanoparticles when a comparison is set with other nanoparticles of different shapes such as rods, bricks and platelets.
VIII. When the laser parameter Ω^* vanishes, the velocity shows symmetry and by enhancing the value of the laser parameter, that behavior is reversed.
IX. The present model can be reduced to a Newtonian model if we set the yield stress $P_y = 0$.
X. The laser radiation enhances the fluid temperature as well as the flow velocity.
XI. In the absence of the laser parameters ($\Omega^* = 0$ and $\gamma^* = 0$) through a clear Newtonian fluid, our results are in good agreement with that obtained by Bandopadhyay et al. [32]

Nomenclature

$(\bar{u}, \bar{v})$	the components of velocity
ρ_e	the density of charge
σ	the electrical conductivity
μ_{hnf}	the viscosity of the hybrid nanofluid
k_{hnf}	the hybrid nanofluid thermal conductivity
ρ_{hnf}	the hybrid nanofluid density
$(\rho C)_{hnf}$	the heat capacitance of hybrid nanofluid
I_0, Ω_0	the laser radiation
γ	the thermal expansion coefficient
$\vec{j}$	the current density for the fluid
E_0	the electric field
B_0	the magnetic field
d	the channel mean-half width
λ	the wavelength
t	the time
a	the amplitude
c	the phase speed of the wave
ρ_e	the density of chargeε the valence of ions

n^+ and n^-	are the density numbers of the positive and negative ions
e	the charge of electron
k_B	the Boltzmann constant
T_{av}	the local absolute temperature of the electrolytic solution
n_0	the bulk volume concentration for the positive or negative ions
K	the Debye–Huckel's parameter that describes the thickness properties of the EDL
$\bar{\varphi}$	the electroosmotic potential function
ϵ	the dielectric constant
q_r	the radiative heat flux
σ'	the constant of Stefan–Boltzmann
k	the coefficient of mean absorption
ϕ_{s1}	the volume fraction for Au nanoparticles
ϕ_{s2}	the volume fraction for Al_2O_3 nanoparticles

Greek symbols

γ^* and Ω^*	are the laser parameters
Da	is the electrical Raleigh number
β	is the non-Newtonian fluid parameter
R_n	is the parameter of chemical reaction
m	is the electroosmotic parameter
Es	is the parameter of electrical field strength
Ha	is the Hartmann number
U_{HS}	is the Helmholtz–Smoluchowski

Disclosure statement

No potential conflict of interest was reported by the author(s).

Funding

The authors express their deep gratitude to The British University in Egypt (BUE) for supporting this work through the Young Investigator Research Grant (YIRG2018-04) awarded to Sara I. Abdelsalam in AY2018-2019.

References

[1] Knott EK. Development of ultraviolet blood irradiation. Am J Surg. 1948;76(2):165–171.
[2] Stulin ID, Lukacher Gla, Teplova LP, Borovikova EN. The dynamics of the cerebral circulation during the treatment of schizophrenics with a depressive syndrome by means of the intravenous laser irradiation of the blood. Zh Nevrol Psikhiatr Im S. S. Korsakova. 1994;94(1):54–56. Russian. PMID:7912026.
[3] Siposan DG, Lukacs A. Effect of low-level laser radiation on some rheological factors in human blood: an in vitro study. J Clin Laser Med Surg. 2000;18(4):185–195.
[4] Maxwell J. A treatise on electricity and magnetism. Cambridge: Oxford University Press; 1904.
[5] Choi S. U.S. Anomalous thermal conductivity enhancement in nanotube suspensions. Appl Phys Lett. 2001;79(14):2252–2254.

[6] Choi S. U.S. enhancing thermal conductivity of fluids with nanoparticles. ASME International Mechanical Engineering congress & exposition. Washington DC: United States,1995; p. 99–105. https://www.osti.gov/servlets/purl/196525
[7] Sadaf H, Abdelsalam SI. Adverse effects of hybrid nanofluid in a wavy nonuniform annulus with convective boundary conditions. RSC Adv. 2019;10:15035–15043.
[8] Bhatti MM, Ellahi R, Zeeshan A, et al. Swimming of motile gyrotactic microorganisms and movement of nanoparticles in blood flow through anisotropically tapered arteries. Front Phys. 2020;8:1–9.
[9] Abdelsalam SI, Bhatti MM. Anomalous reactivity of thermo-bioconvective nanofluid towards oxytactic microorganisms. Appl Math Mech. 2020;41:1–14.
[10] Mekheimer KS, Hasona WM, Abo-Elkhair RE, et al. Peristaltic blood flow with gold nanoparticles as a third grade nanofluid in catheter: application of cancer therapy. Phys Lett A. 2018;382(2): 85–93.
[11] Sohail M, Naz R, Abdelsalam SI. On the onset of entropy generation for a nanofluid with thermal radiation and gyrotactic microorganisms through 3D flows. Phys Scr. 2020;95:045206.
[12] Abdelsalam SI, Bhatti MM. The study of non-Newtonian nanofluid with Hall and ion slip effects on peristaltically induced motion in a non-uniform channel. RSC Adv. 2018;8:7904–7915.
[13] Abdelsalam SI, Bhatti MM. The impact of impinging TiO_2 nanoparticles in Prandtl nanofluid along with endoscopic and variable magnetic field effects on peristaltic blood flow. Multidiscip Model Mater Struct. 2018;14(3):530–548.
[14] Jamshed W, Nasir NAAM, Isa SSPM, et al. Thermal growth in solar water pump using Prandtl–Eyring hybrid nanofluid: a solar energy application. Sci Rep. 2021;11:18704, doi:10.1038/s41598-021-98103-8.
[15] Punith Gowda RJ, Naveen Kumar R, Jyothi AM, et al. KKL correlation for simulation of nanofluid flow over a stretching sheet considering magnetic dipole and chemical reaction. ZAMM. 2021;101; doi:10.1002/zamm.202000372.
[16] Sehra HSU, Shah SIA, et al. Convection heat mass transfer and MHD flow over a vertical plate with chemical reaction, arbitrary shear stress and exponential heating. Sci Rep. 2021;11:4265, doi:10.1038/s41598-021-81615-8.
[17] Ur Rasheed H, AL-Zubaidi A, Islam S, et al. Effects of Joule heating and viscous dissipation on magnetohydrodynamic boundary layer flow of Jeffrey nanofluid over a vertically stretching cylinder. Coatings. 2021;11(3):353, doi:10.3390/coatings11030353.
[18] Ur Rasheed H, Islam S, Khan Z. Computational analysis of hydromagnetic boundary layer stagnation point flow of nano liquid by a stretched heated surface with convective conditions and radiation effect. Adv Mech Eng. 2021;13; doi:10.1177/16878140211053142.
[19] Kang Y, Yang C, Huang X. Electroosmotic flow in a capillary annulus with high zeta potentials. J Colloid Interface Sci. 2002;253(2):285–294.
[20] Ghosal S. Electrokinetic flow and dispersion in capillary electrophoresis. Annu Rev Fluid Mech. 2006;38:309–338.
[21] Ghosh U, Chakraborty S. Electroosmosis of viscoelastic fluids over charge modulated surfaces in narrow confinements. Phys Fluids. 2015;27(6):062004.
[22] Mekheimer KS, Hasona WM, El-Shekhipy AA, et al. Electrokinetics of dielectric non-Newtonian bio fluids with heat transfer through a flexible channel: numerical study. Comput Methods Sci Technol. 2017;23:331–341.
[23] Keramati H, Sadeghi A, Saidi MH, et al. Analytical solutions for thermo-fluidic transport in electroosmotic flow through rough micro-tubes. Int J Heat Mass Transfer. 2016;92:244–251.
[24] Buren M, Jian Y. Electromagnetohydrodynamic (EMHD) flow between two transversely wavy micro parallel plates. Electrophoresis. 2015;36:1539–1548.
[25] Bhatti MM, Zeeshan A, Ijaz N, et al. Mathematical modelling of nonlinear thermal radiation effects on EMHD peristaltic pumping of viscoelastic dusty fluid through a porous medium duct. Eng Sci Technol Int J. 2017;20(3):1129–1139.
[26] Abo-Elkhair RE, Mekheimer KS, Zaher AZ. Electro-magnetohydrodynamic oscillatory flow of a dielectric fluid through a porous medium with heat transfer: brinkman model. BioNanoScience. 2018;8(2):1–13.

[27] Rudraiah N. Effect of a magnetic field on the growth rate of the Rayleigh–Taylor instability of a laser-accelerated thin ablative surface. Laser Part Beams. 2004;22:29–33.
[28] Nisar KS, Bilal S, Shah IA, et al. Hydromagnetic flow of Prandtl nanofluid past cylindrical surface with chemical reaction and convective heat transfer aspects. Math Probl Eng. 2021; doi:10.1155/2021/5162423.
[29] Ur Rasheed H, Islam S, Khan Z, et al. Numerical solution of chemically reactive and thermally radiative MHD Prandtl nanofluid over a curved surface with convective boundary conditions. ZAMM. 2021; doi:10.1002/zamm.202100125.
[30] Nadeem S, Ijaz S. Influence of metallic nanoparticles on blood flow through arteries having both stenosis and aneurysm. IEEE Trans Nanobioscience. 2015;14(6):668–679.
[31] Mekheimer KS, Zaher AZ, Hasona WM. Entropy of AC electro-kinetics for blood mediated gold or copper nanoparticles as a drug agent for thermotherapy of oncology. Chin J Phys. 2020;65:123–138.
[32] Bandopadhyay A, Tripathi D, Chakraborty S. Electroosmosis-modulated peristaltic transport in microfluidic channels. Phys Fluids. 2016;28(5):052002, doi:10.1063/1.4947115.